Available online at www.sciencedirect.com
ScienceDirect
Acta Materialia 56 (2008) 580–592
Acta MATERIALIA
www.elsevier.com/locate/actamat

A further step towards an understanding of size-dependent crystal plasticity: In situ tension experiments of miniaturized single-crystal copper samples

D. Kiener [a,b,*], W. Grosinger [a], G. Dehm [a,c], R. Pippan [a]

[a] *Erich Schmid Institute of Materials Science, Austrian Academy of Sciences, Leoben, Austria*
[b] *Materials Center Leoben, Forschungs GmbH, Leoben, Austria*
[c] *Department of Materials Physics, Montanuniversität Leoben, Leoben, Austria*

Received 14 August 2007; received in revised form 4 October 2007; accepted 9 October 2007
Available online 3 December 2007

Abstract

A method for in situ testing of miniaturized tension specimen was developed. The size effects of the plastic deformation behavior of copper single crystals loaded along the $\langle -2\,3\,4\rangle$ direction were investigated. The diameter was varied between 0.5 μm and 8 μm, and the aspect ratio, gauge length to side length, between 1:1 and 13.5:1. At high aspect ratios hardening was negligible. However, an increase of the flow stress with decreasing diameter was observed. This increase was small for diameters above 2 μm, and somewhat larger below 2 μm. These findings are explained by individual dislocation sources which govern the plastic deformation. For low aspect ratios the behavior is significantly different. A pronounced hardening and a very strong size effect was observed. Both are a result of dislocation pile-ups due to the constrained glide of the dislocations caused by the sample geometry.

Keywords: Tension test; Copper; Plastic deformation; Size effects

1. Introduction

In the past few years, the deformation of miniaturized single-crystal samples was frequently investigated to examine the processes governing deformation on the micrometer and nanometer length scale. The employed testing methods differ significantly in the stress state of the tested volume. Uchic et al. [1] developed a method to fabricate miniaturized compression samples using a focussed ion beam (FIB) microscope and loaded these columns using a nanoindenter equipped with a flat diamond tip. With this approach, most of the constraints present, for example, in nanoindentation experiments, were removed and the sample was exposed to a nominally uniaxial stress and strain state. The key result of these miniaturized compression experiments was an unexpected size effect in terms of an increased flow stress with reduced sample diameter. The nature of this effect is still under discussion. Nevertheless, this method has to deal with problems due to constraints rising from friction, the limited sample aspect ratio in order to prevent buckling, and the compliance of the sample base. Further uncertainties are induced from the alignment between the sample and the indenter [2].

In the macroscopic world, tension experiments offer several benefits when compared to compression tests. For example, there is almost no limitation to high aspect ratios. In the microscopic world, problems arise due to the difficulties of sample fixation. Therefore, we developed a method to fabricate miniaturized tension samples and individually designed indenter tips serving as tensile sample holders using a FIB, giving us the possibility to systematically

---

[*] Corresponding author. Address: Erich Schmid Institute of Materials Science, Austrian Academy of Sciences, Leoben, Austria. Tel.: +43 3842 804 112; fax: +43 3842 804 116.
E-mail address: dkiener@unileoben.ac.at (D. Kiener).

1359-6454/$30.00 © 2007 Acta Materialia Inc. Published by Elsevier Ltd. All rights reserved.
doi:10.1016/j.actamat.2007.10.015

investigate the origin of mechanical size effects in the micron and sub-micron regime. Furthermore, loading of the tension samples was performed in situ using a micro-indenter mounted in a scanning electron microscope (SEM). Beside high accuracy in local positioning, this approach also provides insight into the deformation process.

In the present manuscript we investigate the tensile deformation of single-crystal copper specimens. The influence of sample size and aspect ratio on the plastic deformation behavior is observed in situ in the SEM and correlated to the measured stress–strain curves. The aim of this study is to improve knowledge of the geometrical aspects governing mechanical properties in the micrometer and sub-micrometer regime.

2. Experimental

Rods with dimensions of 20 mm × 0.5 mm × 0.5 mm were cut from a copper single crystal using a diamond wire saw, in a way so that the $\langle -234 \rangle$ crystal direction is aligned with the length axis of the samples. These rods were mounted on copper holders to simplify further handling and to ensure accurate alignment for the FIB shaping and the following mechanical testing. Subsequently, these rods were electrolytic-polished in phosphoric acid to remove the deformation layer from the cutting process. Additionally, the samples were shaped in the form of a needle with an opening angle of ~30° and a tip radius in the order of several micrometers. This was achieved by moving the samples periodically in and out of the electrolyte. An example of such a needle is presented in Fig. 1a. Tension specimens were prepared from these needles by ion-milling, using a FIB (Zeiss 1540 XB) with a Ga^+ ion source operated at an acceleration voltage of 30 kV under perpendicular ion impact, as displayed in Fig. 1b–d. For this purpose, in a first step two parallel sides were coarse-shaped with an ion current of 1 nA (Fig. 1b). Then the sample holder was rotated by 90° around the length axis of the needle and the other two sides were cut from the lamella produced in the first step (Fig. 1c), the applied ion current for coarse milling was again 1 nA. The final shaping to the desired dimensions was performed with an ion current of 100 pA in order to reduce the ion-induced damage [3]. Subsequently, the sample was rotated back to the initial orientation for the final shaping of these two sides (Fig. 1d), again using an ion current of 100 pA. This was necessary to ensure that redeposition during the second milling step does not influence the desired sample dimensions or mechanical properties. For the investigated samples, the $\langle -234 \rangle$ axis of the single crystal was parallel to the loading direction, side lengths, a, ranging from

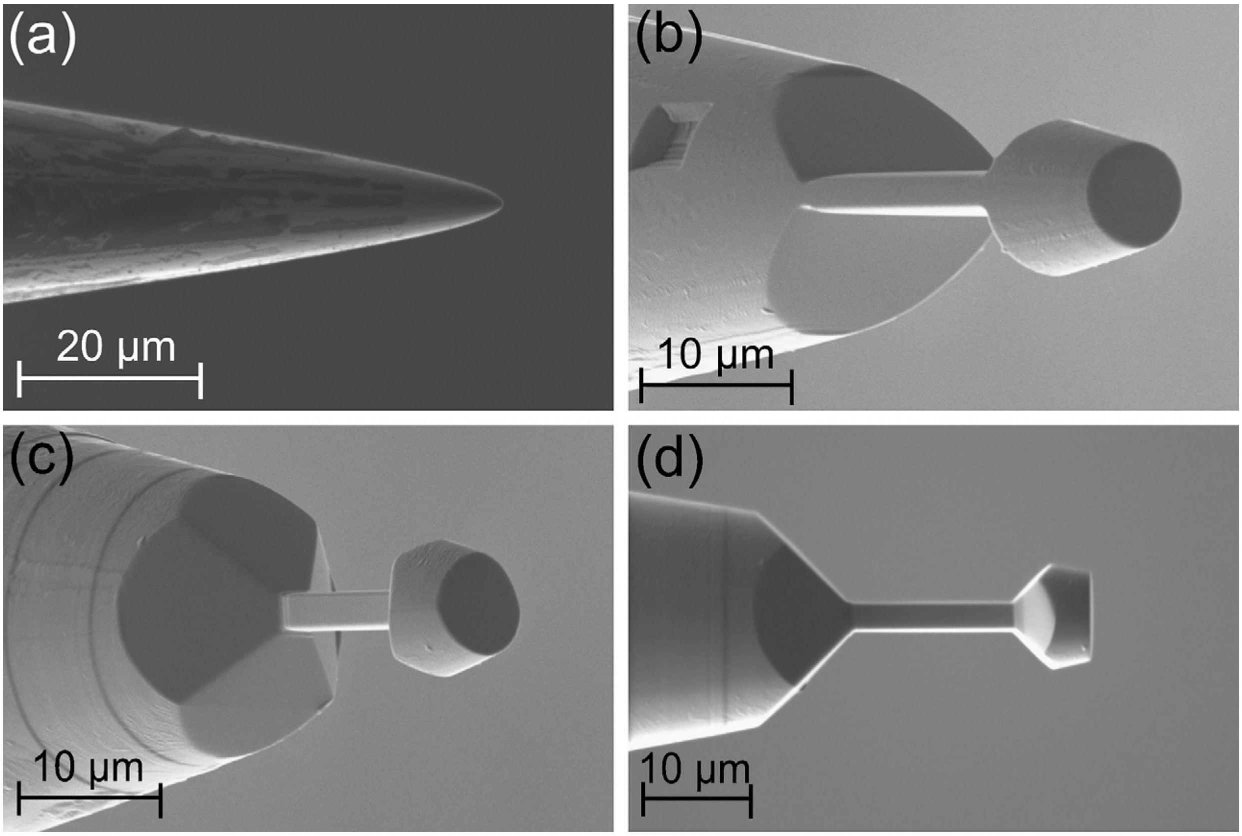

Fig. 1. (a) Single-crystal copper needle with $\langle -234 \rangle$ crystal direction along the length axis after electrolytic thinning. (b) FIB milling of first two parallel side planes. (c) Shaping of the other two perpendicular side planes after rotating the sample by 90° around the length axis. (d) Final shape of a tension sample with a side length $a = 3$ μm and an aspect ratio of 5:1. Note that (b and c) are inclined views.

0.5 μm to 8 μm, and aspect ratios defined as gauge length/side length between 1:1 and 13.5:1.

Immediately after FIB milling was finished, tensile testing was conducted under vacuum conditions (vacuum pressure $\sim 2 \times 10^{-6}$ mbar) to avoid the formation of extensive oxide layers on the sample surface. The time the specimens were exposed to humid air was kept below a few minutes. This time was necessary to vent the FIB chamber, manipulate and transport the specimen between the different devices, and evacuate the SEM chamber. The samples were loaded using a microindenter (ASMEC UNAT) mounted inside an SEM (LEO Stereoscan 440). This indenter was equipped with special dovetail-shaped tips serving as sample gripper to ensure form-closed connection between sample and indenter. These grippers were fabricated from polycrystalline tungsten needles, which are usually employed in micromanipulators, again by FIB machining. Differently sized grippers were used for the differently sized tension samples to ensure that there is sufficient contact area between sample head and sample gripper when using self-similar specimen. An example is shown in Fig. 2a, presenting an SEM image of the same sample as shown in Fig. 1 along with the corresponding sample gripper. A major advantage of the employed in situ setup is the highly precise alignment, enabled by direct visual control. Otherwise it would be impossible to perform the four-axis operations necessary to position the tension sample in a way that the flanks of the sample head are parallel and equally spaced from the flanks of the sample gripper, as illustrated in Fig. 2b. It is acknowledged that there is an uncertainty in the alignment of the length axis of sample and gripper in the *z*-direction. By knowing the dimensions of the gripper, this can be adjusted with an accuracy of ±1 μm. Therefore, we do not expect that out-of-plane loading of our specimen will influence our results.

The samples were loaded in open displacement controlled mode to engineering strains larger than 15%. During tensile testing, load and displacement were measured. Furthermore, sequences of SEM images were recorded and analyzed together with the load–displacement data.

3. Results

3.1. Method

Fig. 3a shows the load–displacement data collected for the tension sample with $a = 3$ μm and an aspect ratio of 5:1. Positioning of the tensile specimen was conducted in a way such that there was always a small slit of the order of one micron between the flanks of the sample and the gripper. This is to prevent any contact before loading. Therefore, the graph shows a regime without load where the sample gripper approaches the sample. The noise present in this regime gets significantly reduced once the sample and the gripper are in full contact in the regime of linear loading, as can be seen in the inset in Fig. 3a. Beside a serration-like behavior, the load–displacement curve exhibits several pronounced load drops, corresponding to the appearance of distinct glide steps during in situ monitoring. Furthermore, it is obvious from this data as well as the in situ observation that despite all taken effort the contact between the sample and the gripper flanks is not perfect and there is a region of surface adaptation before the linear loading regime.

To calculate technical stress–strain curves from the load–displacement data, the load was simply divided by the initial cross-section determined after final shaping of the sample in the FIB. To calculate strains, the linear loading regime was extrapolated to intersect the axis of abscissae and the contact-free part of the load–displacement curve (including the surface adaptation regime) was omitted. The corresponding stress–strain curve calculated from the load–displacement data of Fig. 3a is presented in Fig. 3b. After unloading, this sample was reloaded a second time (dotted arrows in Fig. 3b). Two important aspects will be mentioned. First, the reload starts with a linear regime. Second, upon reloading the flow curve continues

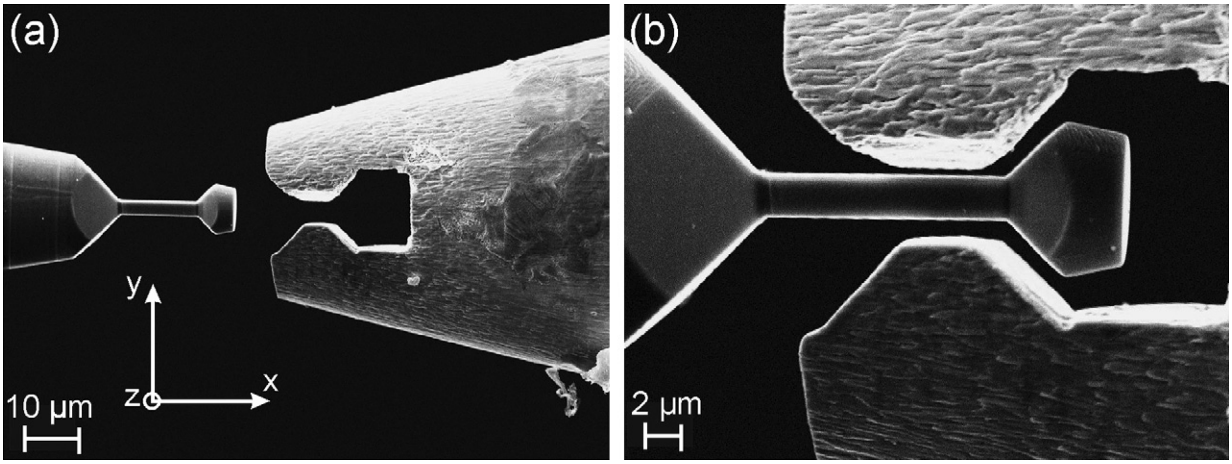

Fig. 2. (a) SEM image showing a single-crystal copper tension sample and the corresponding tungsten sample gripper before the test at a low magnification. (b) Sample and gripper aligned prior to loading. The loading direction is along ⟨−234⟩.

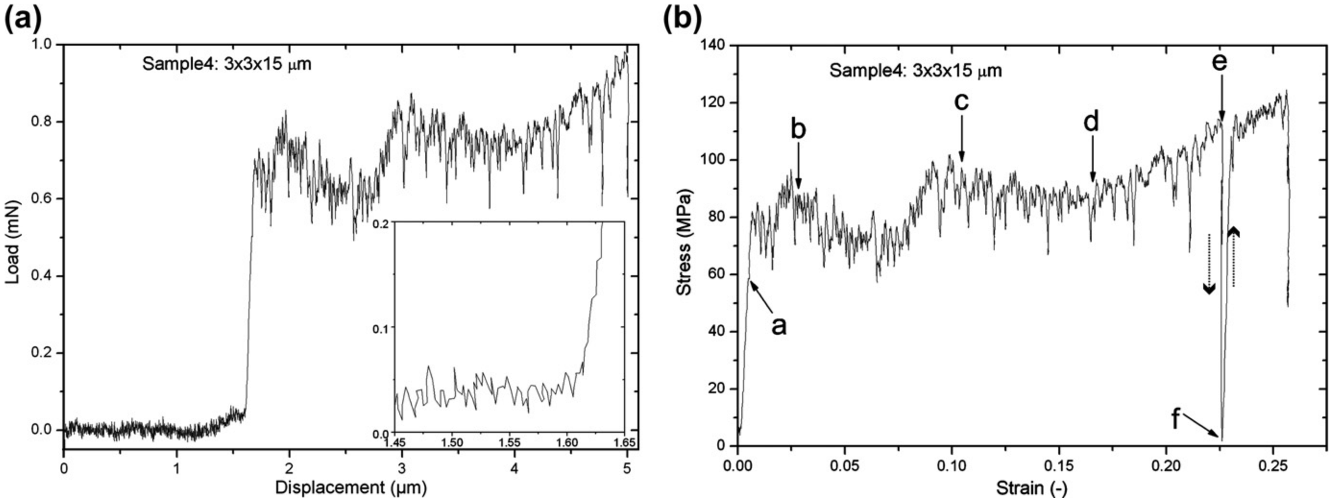

Fig. 3. (a) Load–displacement curve measured for the first loading of the sample depicted in Fig. 2. The inset shows details of the measured curve just before full contact between the sample and the gripper is established. (b) Stress–strain curve calculated from the load–displacement data. A second loading step (indicated by dotted arrows) performed for this sample is included in the graph but not shown in (a). See text for details.

from the stress level where it ended before unloading. This statement holds true for the load–displacement curves of all further loading steps, indicating that the contact sites were already adapted after the first loading.

Fig. 4 shows in a series of SEM images the formation of distinct glide steps first in the center of the sample (Fig. 4b), and finally along the whole gauge length (Fig. 4c–e). The corresponding positions along the stress–strain curve are

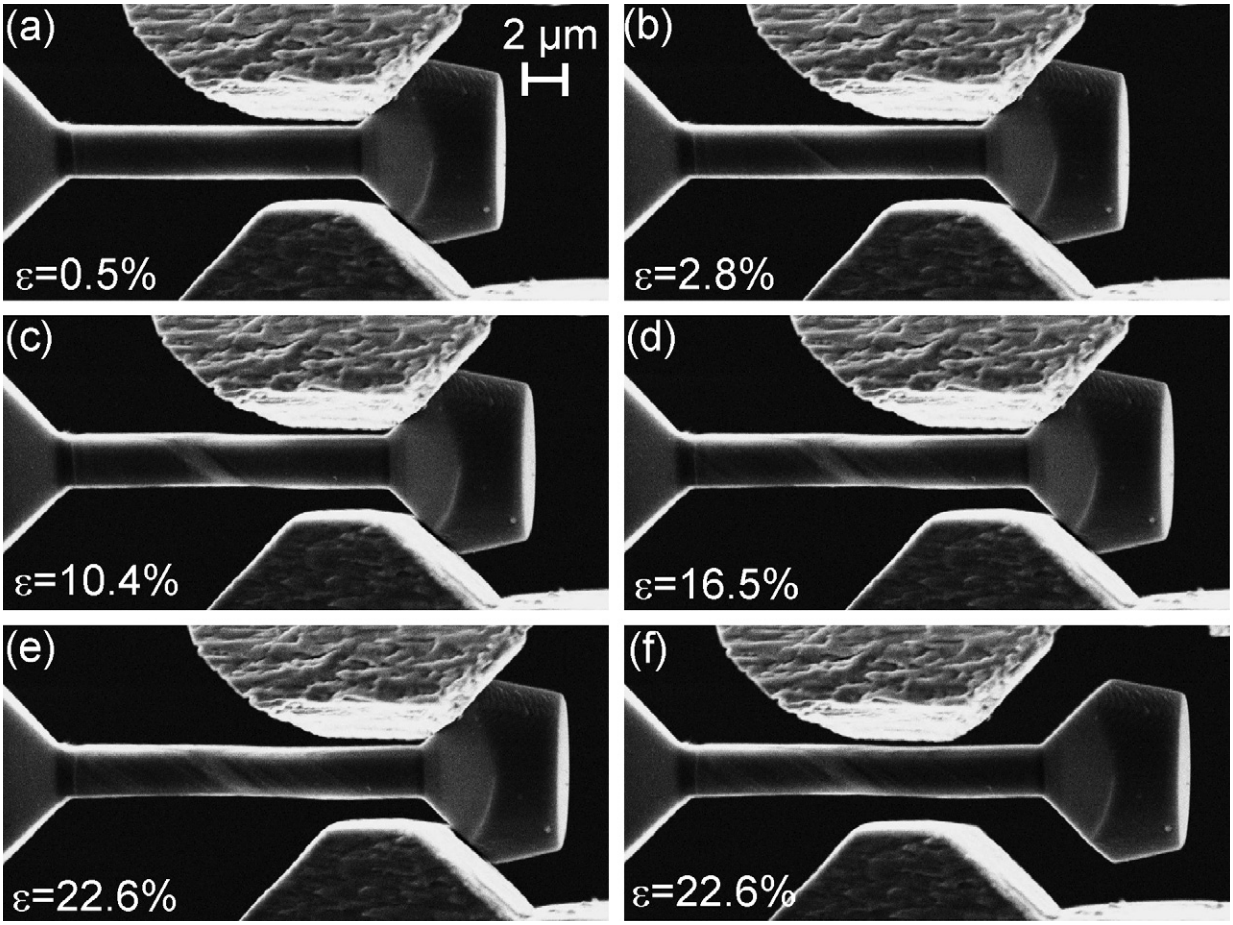

Fig. 4. SEM images of the sample shown in Fig. 2 taken during in situ tensile testing (a–e) and after unloading (f). The corresponding positions along the stress–strain curve are indicated by arrows in Fig. 3b.

indicated by arrows in Fig. 3b. Fig. 4f shows the sample and the gripper after unloading.

3.2. Geometrical constraints

To investigate the influence of the gauge length, samples with $a = 3$ μm and an aspect ratio of 5:1 were fabricated. These were confined in the middle of the gauge length to dimensions of $1.5 \times 1.5 \times 8$ μm, $1.5 \times 1.5 \times 1.5$ μm with an opening angle of the flanks of 45°, and $1.5 \times 1.5 \times 1.5$ μm with an opening angle of 90°, respectively. SEM images of these samples taken during tensile testing are shown in Fig. 5.

While the unconfined sample with the high aspect ratio of 5:1 (Fig. 5a) shows pronounced glide steps distributed over the whole sample length, these features are strongly reduced in the case of the confined samples with an aspect ratio of 1:1. Whereas in the case of the 45° flanks (Fig. 5b) some glide steps are visible, they are even less distinct for the sample with the 90° flanks (Fig. 5c).

The corresponding stress–strain curves shown in Fig. 6 reflect this observation, with the flow stresses of the confined samples being significantly higher than the unconfined one (roughly by a factor between 2 and 3). Furthermore, the confined sample with the 90° flanks displays higher stress levels than the confined sample with the 45° flanks. It is acknowledged that the initial loading slopes of the three samples are different, with the most constrained sample having the lowest slope. This aspect will be further discussed in the Appendix.

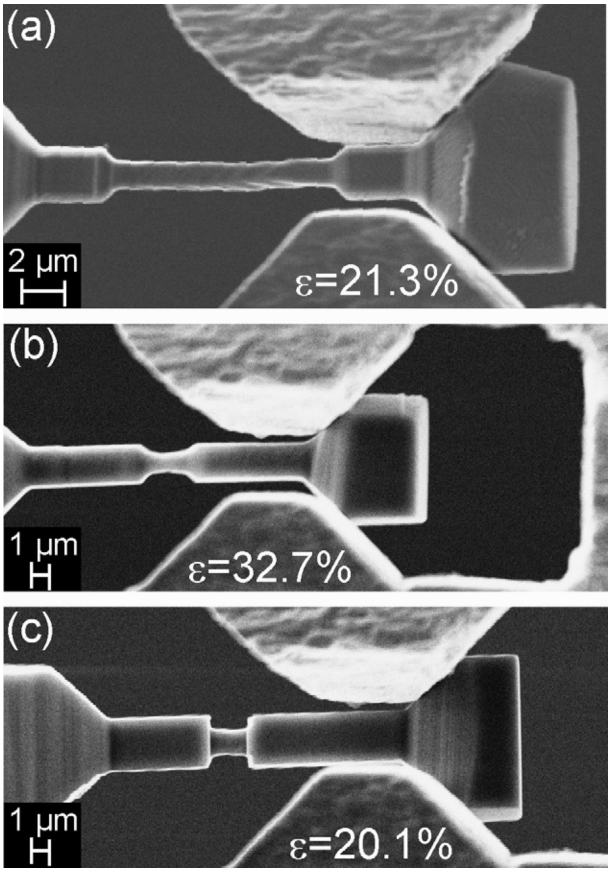

Fig. 5. SEM images taken during in situ loading of miniaturized copper tension samples with $a = 1.5$ μm and aspect ratios of (a) 5:1 and (b and c) 1:1, respectively. To further constrict deformation for the samples with an aspect ratio of 1:1, the flank angle was changed from (b) 45° to (c) 90°.

3.3. Pre-straining

The influence of pre-straining on the mechanical response was investigated in a further experiment. Therefore, a sample with $a = 8$ μm and an aspect ratio of 5:1 was strained to 5.4% (Fig. 7a and b). Subsequently, the specimen was reduced by FIB milling to $a = 3$ μm over the whole sample length, resulting in an aspect ratio of 13.5:1. This sample was afterwards again loaded to strains above 10%.

The stress–strain curves of these two specimens are shown in Fig. 8. The smaller, pre-strained sample exhibits a higher stress to initiate deformation. At higher strains, the stress levels are not far apart. In both cases, deformation in terms of visible glide steps started near the sample center (see arrows in Fig. 7a and c) and expanded along the gauge length.

3.4. Size effects

Finally, the technical stress–strain curves of all samples discussed in this investigation are shown in Fig. 9. There is no significant hardening found for the samples with an aspect ratio of 5:1 or higher, while the sample with $a = 8$ and an aspect ratio of 1:1 exhibits significant hardening.

In order to give an overview and ease comparison to other investigations, the size-dependent flow stress at 10% strain is shown in Fig. 10. The open symbols reflect samples with an aspect ratio of 5:1, while the filled symbols correspond to samples with an aspect ratio of 1:1. As indicated in Fig. 7e the pre-strained sample with $a = 3$ μm and an aspect ratio of 13.5:1 was fabricated from a tested sample with $a = 8$ μm and an aspect ratio of 5:1. The two corresponding data points are marked by an arrow. Furthermore, this thicker sample serving as pre-form was strained to only 5.5% (Fig. 8). Therefore, the stress at 5% strain is included in Fig. 10. The magnitude of the error bars will be discussed in the Appendix.

4. Discussion

The experimental challenges and factors affecting such miniaturized tension experiments are discussed in the Appendix. In this section the attention is mainly focussed on the plastic flow behavior of the miniaturized single-crystal tension samples.

4.1. High aspect ratios (5:1 and higher)

The presented images taken from the in situ experiments showed that slip takes place in clearly defined planes

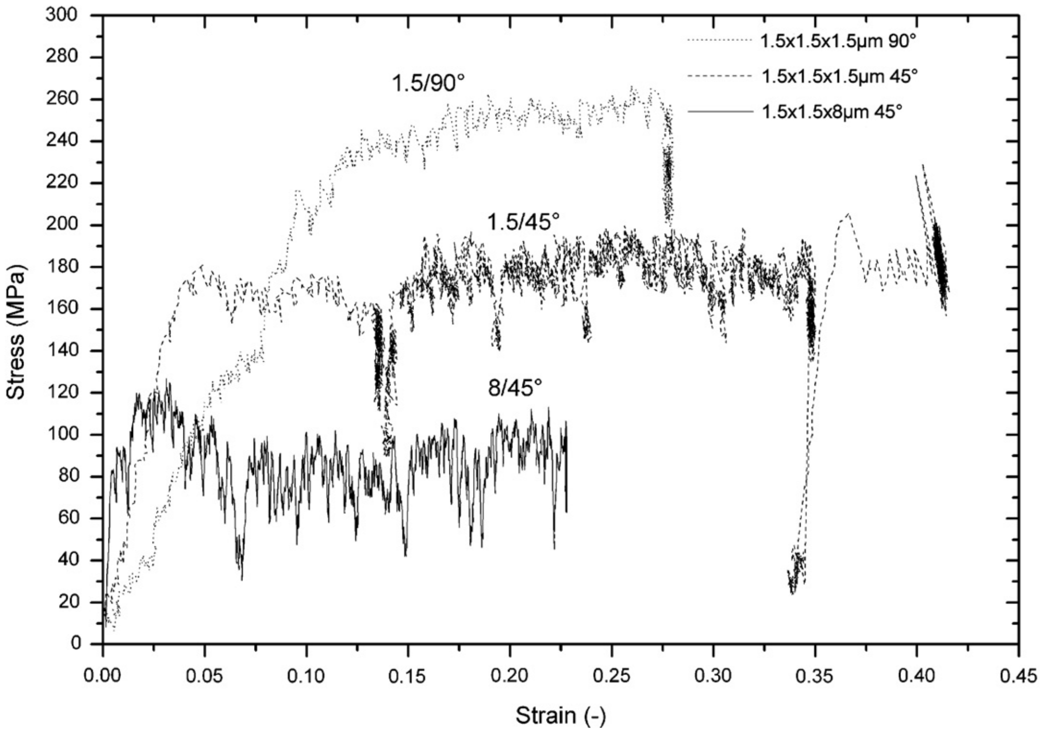

Fig. 6. Stress–strain curves measured for the samples displayed in Fig. 5. Strong influence of the geometrical confinement on the mechanical behavior is present, with the geometrically more constricted samples showing significantly higher flow stresses.

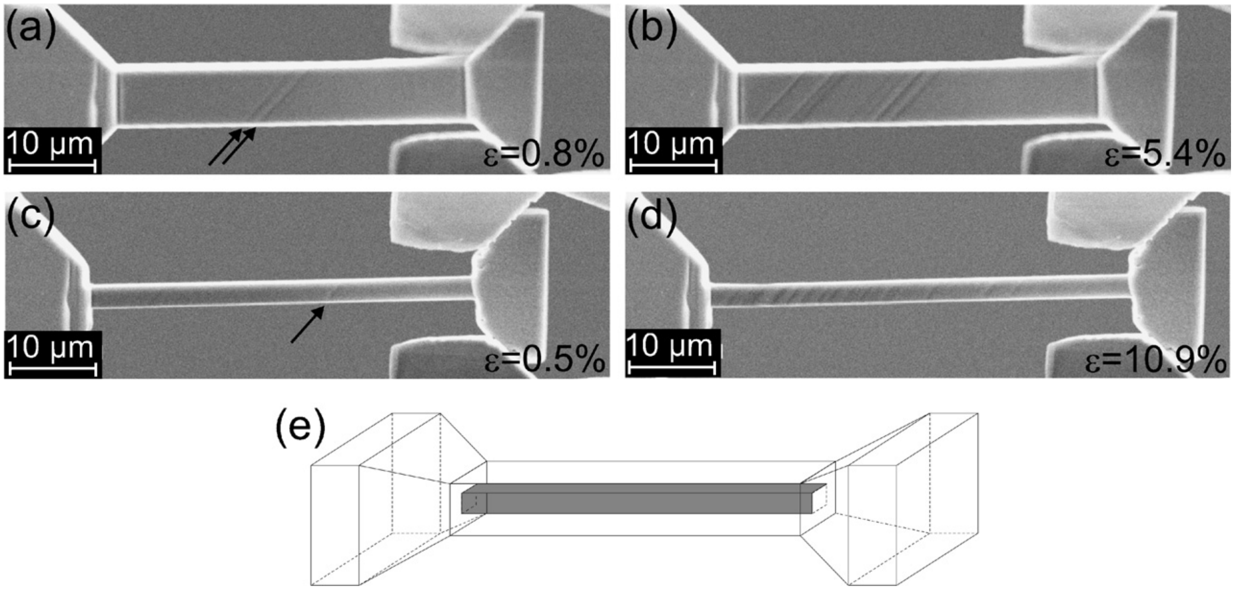

Fig. 7. SEM images taken during in situ tensile testing of a sample with $a = 8$ µm (a and b). After straining to 5.5%, this sample was FIB machined to $a = 3$ µm and loaded again (c and d). First emerging glide planes are indicated by arrows. A schematic of the specimen reduction is presented in (e).

throughout the whole sample. This is also depicted in the high-resolution SEM image taken after deformation of the sample displayed in Fig. 4. Despite the high total strain of more than 25%, there is only one type of glide step visible on the surface (see Fig. 11a). Furthermore, no indication of necking was found, supporting the assumption of single slip deformation. To further confirm the finding of single slip, the local crystal orientations were investigated using electron backscatter diffraction (EBSD). Fig. 11b presents an inclined view of the sample with an overlay indicating the local crystal orientation in transverse direction (TD). The insets represent the applied color code and the (1 0 0) pole figure calculated from this data, respectively. No peak broadening or streaks were observed. The higher magnified

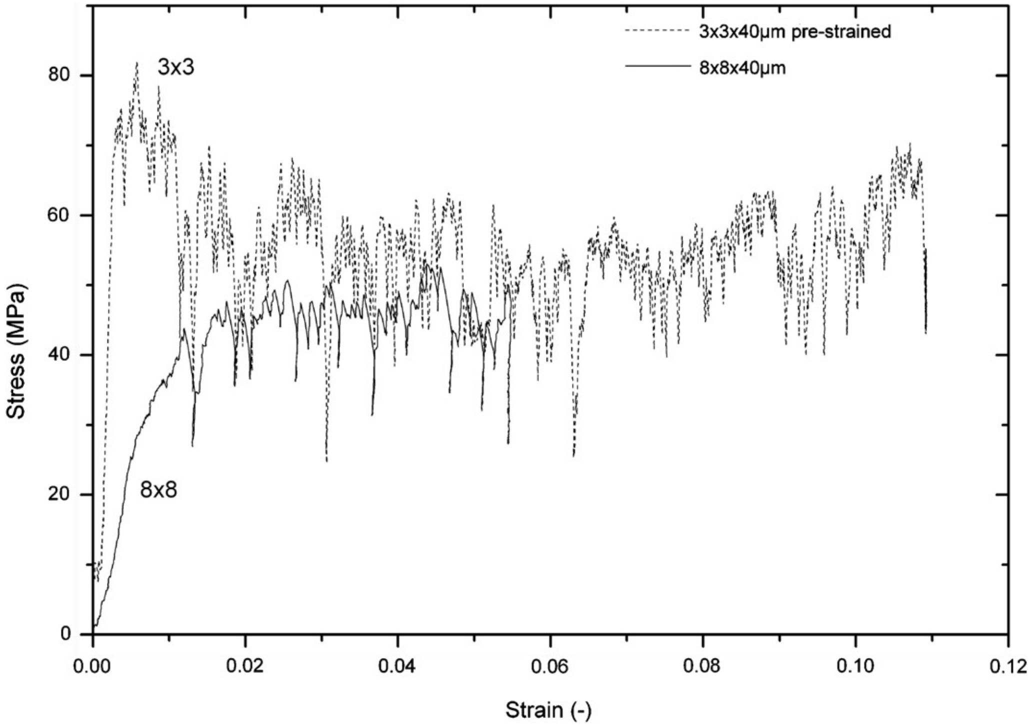

Fig. 8. Stress–strain curves of the 8 × 8 × 40 μm sample depicted in Fig. 7a and b, and the 3 × 3 × 40 μm sample FIB milled from this already strained specimen, depicted in Fig. 7c and d.

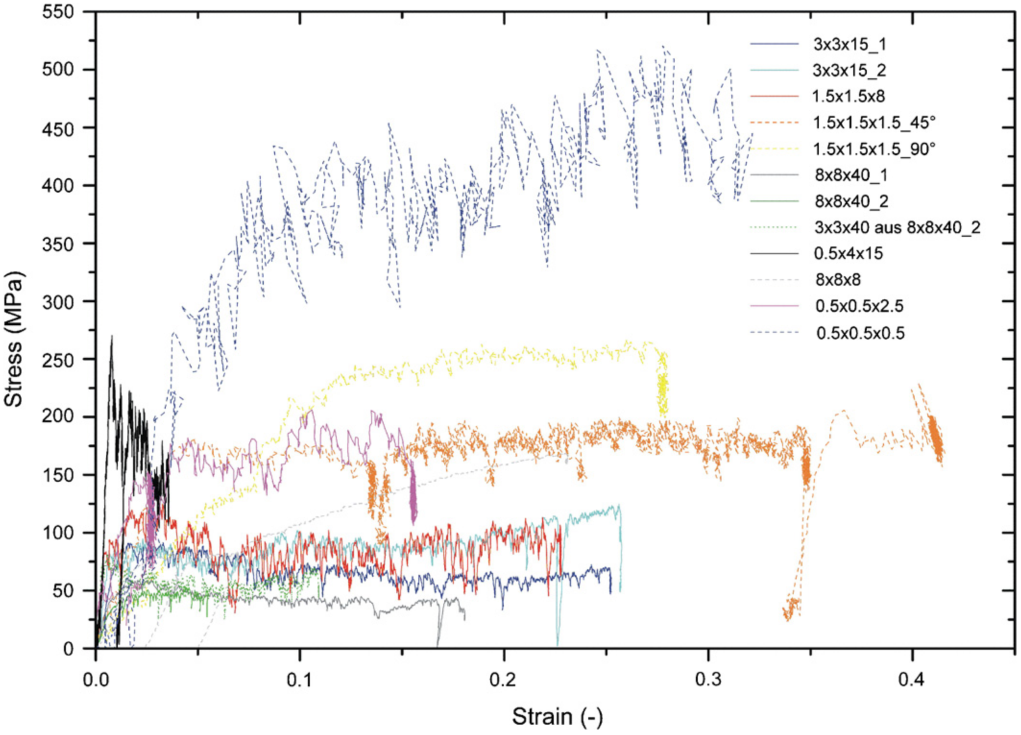

Fig. 9. Technical stress–strain curves of miniaturized single-crystal copper tension samples loaded along the ⟨−234⟩ crystal direction. Full lines indicate an aspect ratio of 5:1, dashed lines reflect an aspect ratio of 1:1, and a dotted line indicates a pre-strained specimen.

EBSD scan (Fig. 11c) depicts no distinct misorientations. The zone in the center of the sample could not be measured due to shadowing effects. A misorientation profile along the sample length, calculated with respect to the starting point of the profile, indicated in Fig. 11c, shows a slight rise in misorientation from ~0.5° (which is the accuracy of the system)

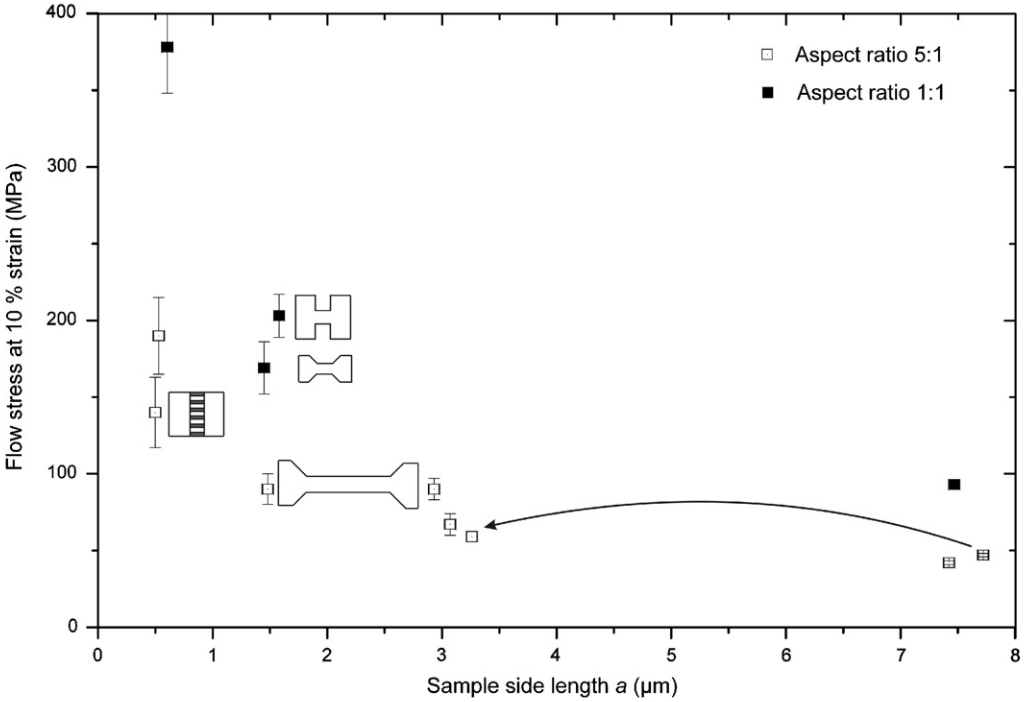

Fig. 10. Size-dependent technical flow stress of miniaturized copper tension specimens loaded along the $\langle -2\,3\,4\rangle$ direction at a strain of 10% extracted from Fig. 9. For several samples the error bars are smaller than the used symbol. See text for details.

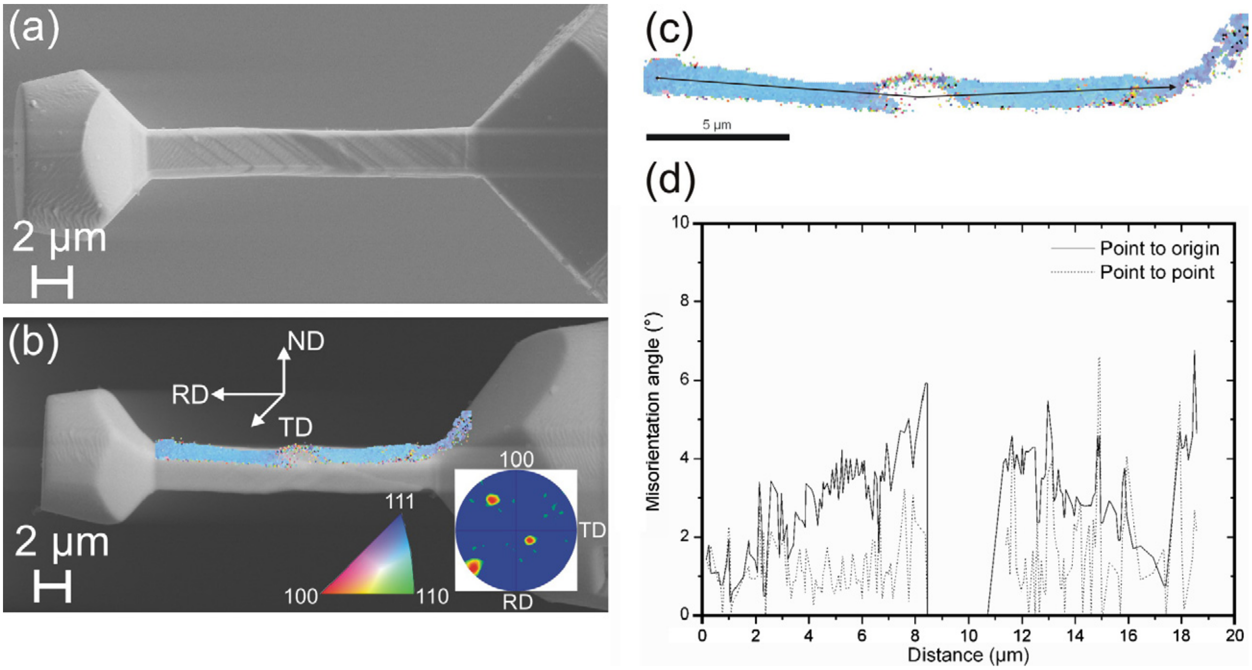

Fig. 11. (a) High-resolution SEM image presenting the deformed tension sample of Fig. 4. Only one set of glide steps is visible. (b) EBSD scan indicating the local crystal orientation in transverse direction (TD) along the sample. The insets present the applied color code and the (1 0 0) pole figure calculated from the EBSD data. (c) Higher magnified EBSD data. (d) Misorientation profile along the path shown in (c). See text for details.

at the left end of the sample to ~5° at the sample center. Following the region without measured orientations, this value decreases down to ~0.5° again and rises slightly when approaching the sample flanks. These misorientations stem from the global deformation of the sample. No gradients in misorientation corresponding to a pile-up of dislocations or storage of dislocations during deformation [4] were found in the gauge length.

The fact that single slip takes place over the whole sample length leads to the conclusion that a number of single sources controls the plastic flow. Each source is responsible for a certain plastic deformation or induces an avalanche on the corresponding slip plane, subsequently followed by the activation of the next source. It is supposed that this change takes place as a consequence of the redistribution of local stresses, mainly because the fixed sample ends can cause a local bending stress. No significant hardening except the serration-like behavior was observed. This implies that there is no building up of forest dislocations.

The measured flow stress is significantly lower than in other small-scale experiments (compression [1,5], bending [4,6], indentation [7,8], ...). Nevertheless, a size effect is observed with the flow stress at 10% strain rising from ~40 MPa for $a = 8$ μm to ~170 MPa for $a = 0.5$ μm.

Assuming that the source size determines the flow stress, one can calculate this source size from the measured stresses by applying [9]

$$\tau_{\text{source}} = \frac{Gb}{2\pi} \cdot \frac{1}{S} \cdot \ln\left(\frac{\alpha \cdot S}{b}\right) \tag{1}$$

where $G = 47$ GPa is the bulk modulus, $b = 2.56 \times 10^{-10}$ m is the Burgers vector, S is the length of the source, and α is a numerical constant in the order of unity. This equation is valid for a Frank–Read source with size S (the U-mill following the nomenclature by Orowan [10]) or a single-ended source with size $S/2$ (the L-mill) [11].

The result of these calculations is depicted in Fig. 12a for an L-mill. τ_{source} was obtained by converting the flow stresses at 1% strain to shear stresses by assuming glide on the {111} plane with the highest Schmid factor $m_{-234} = 0.422$ for the given configuration. An increase in source size from $S_L \sim 500$ nm for $a = 0.5$ μm to $S_L \sim 2000$ nm for $a = 8$ μm is observed (Fig. 12). The effect of image forces from the free surface is negligible in these dimensions and was therefore not taken into account.

To understand why the sample size should dominate the source size, one has to consider the glide geometry of the investigated specimen as schematically depicted in Fig. 12b. Every U-mill will end up as two L-mills after first activation [12]. Therefore, we assume this type of dislocation source to be the typical deformation mechanism in our experiments. As our glide planes have a rectangular shape, there is a periodic variation of the source length. The flow stress is hence determined by the minimal source length, which scales with the sample diameter. There must not necessarily be a U-mill present in the sample to generate the L-mill, also the partial removal of an initial dislocation source during FIB milling produces a single dislocation arm, which can operate in the depicted way.

Furthermore, during operation the free dislocation end will periodically not only change in length but also in character between edge and screw. The difference in line energy between screw dislocation and edge dislocation is given by [13]

$$E_{\text{L,edge}} = \frac{E_{\text{L,screw}}}{1 - \nu} \tag{2}$$

Additionally, if the penetration point of the dislocation on the surface is of edge character, lattice relaxation takes place in this area, resulting in an additional pinning force on the dislocation end, leading to an extra curvature of the dislocation line.

Finally, there is a stress contribution, σ_{ledge}, due to the ledge formation energy of the screw dislocation emerging on the surface, which is dependent on the sample size in an inverse manner [14]

$$\sigma_{\text{ledge}} = \frac{1}{m} \cdot \tau_{\text{ledge}} = \frac{1}{m} \cdot \frac{2\gamma}{a} \tag{3}$$

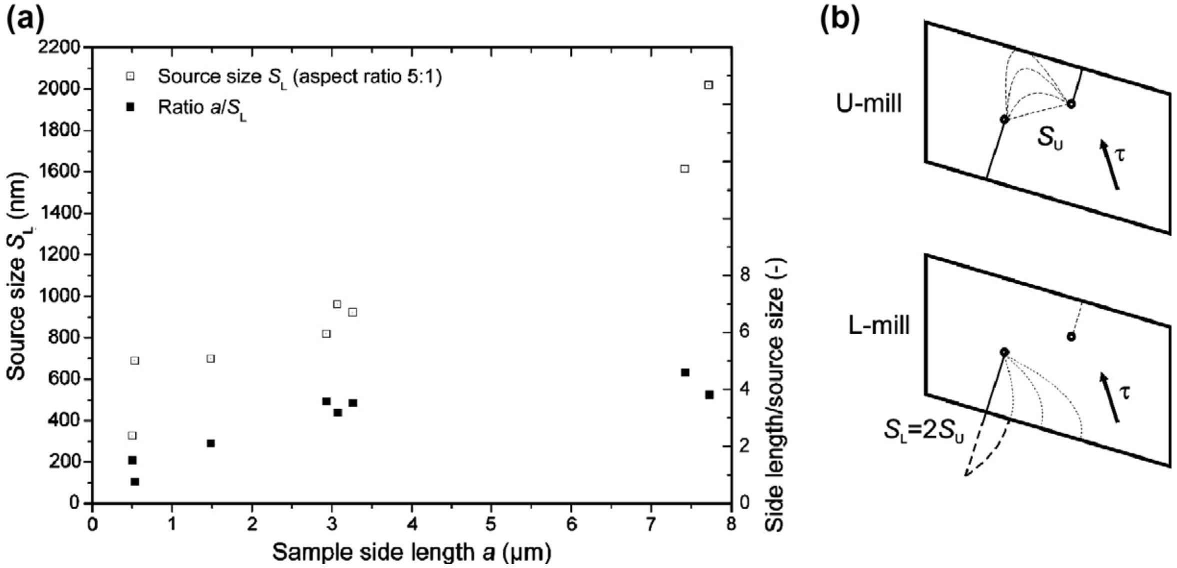

Fig. 12. (a) Calculated dependence of source size S_L and ratio a/S_L on the sample side length a for a L-mill using Eq. (1). (b) Schematic view on the glide plane of a tension specimen showing the first operation of a U-mill and the subsequent operation of the longer arm of the generated L-mill.

where $\gamma = 1.69\ \mathrm{J\ m^{-2}}$ is the surface energy of copper [14], $m = 0.422$ is the Schmid factor, and a is the sample side length.

For sample side lengths of 0.5 μm, 1 μm, and 2 μm this leads to a σ_{ledge} of 16 MPa, 8 MPa, and 4 MPa, respectively. This is a small contribution in the investigated regime, but becomes important upon further decrease of the specimen size.

There are other aspects like the presence of an oxide layer or the FIB damaged layer to be considered. However, we do not expect them to have a significant effect on the plastic flow behavior, as in that case the stress should drop significantly after this layer is cut by the first emerging glide step. This was not observed in our experiments. Furthermore, if a layer would be present one would expect the deformation to continue on the plane where this layer was broken. Contrary, our samples showed several distinctive glide steps (Fig. 13a). A schematic of this cutting process is presented in Fig. 13b. Note that the thickness of the oxide layer/FIB damaged layer is overdrawn. Detailed investigations on the FIB damaged layer and possible mechanical consequences are reported elsewhere [3]. Fibre tensile testing experiments of electrolytically thinned copper wires with diameters ranging from 50 μm down to 15 μm report flow stresses for the smallest wire which are in good agreement with our data [7].

Comparison of our results with tension experiments of bulk single-crystal copper shows that the observed stresses are higher than the orientation-dependent stresses between 1 and 2 MPa reported by Diehl [15] for stage I deformation of macroscopic single-crystal copper. Whether this difference stems from different dislocation densities, impurity contents, the presence of pre-existing forest dislocations, or the "constrained" tension experiment (our sample gripper suppresses movement of the tension sample in the y-direction [15]), is not clear and subject to further investigations.

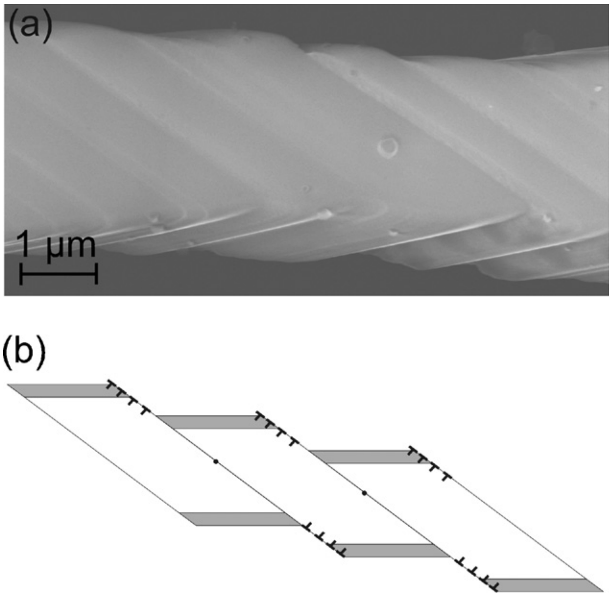

Fig. 13. (a) High-resolution SEM image of a tension sample with $a = 3$ μm and an aspect ratio of 5:1 taken after a deformation of 25.1%. Distinct glide steps are visible on the sample surface. (b) Schematic demonstrating the negligible effect of an oxide or FIB damaged layer on the flow stress after emerging of large glide steps.

4.2. Low aspect ratio (1:1)

When performing macroscopic tensile tests, a reduction of the aspect ratio causes a small increase of the flow stress due to the development of a multiaxial stress state, like in the neck of a long tensile specimen. In the case of the miniaturized tension samples, a significant effect on the flow stress is observed, which is more pronounced than for the samples with high aspect ratio. Furthermore, these samples exhibit strong hardening contrary to the samples with high aspect ratio.

The inclination angle of the glide plane in combination with the chosen sample geometry prevents simple glide of the dislocations over the sample cross-section (Fig. 14a). Therefore, the dislocations glide into the shoulder of the tension samples (Fig. 14b). The cross-section in this shoulder region increases significantly, reducing the shear stress approximately by an order of magnitude for the sample with 90° shoulders, and by the equations given in Fig. 14b in the case of 45° shoulders. Thus, the shear stress rapidly drops below the level necessary to move dislocations. Consequently, pile-ups form at the end of the tension samples. These pile-ups were confirmed by EBSD scans showing distinct misorientations.

The required number of edge-type dislocations Δn in a pile-up to reach the measured stress levels with respect to the sample with an aspect ratio of 5:1 can be estimated as [13]

$$\Delta n = \frac{L(1-\nu)}{Gb} \cdot \Delta\tau \tag{4}$$

where L is the length of the pile-up, which was assumed to be half the glide plane length, $\nu = 0.28$ is Poisson's ratio, and $\Delta\tau$ the rise in shear stress.

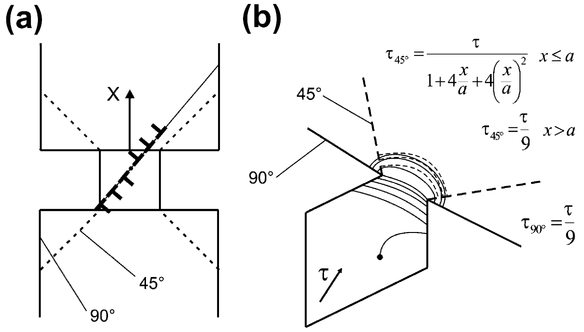

Fig. 14. (a) Schematic of the short tension samples indicating that no free glide plane exists. (b) View on the glide plane showing the pile-up emerging for both geometries. The provided equations give the shear stress present in the shoulder part of the tension sample for the 45° geometry ($\tau_{45°}$) and the 90° geometry ($\tau_{90°}$), respectively.

Regarding the sample with $a = 8\ \mu\text{m}$, taking $\Delta\tau_{8,45^\circ} \sim 30$ MPa leads to a number of $\Delta n_{8,90^\circ} \sim 27$ dislocations in the pile-up. The sample with $a = 1.5\ \mu\text{m}$ and the 45° flanks exhibited $\Delta\tau_{1.5,45^\circ} \sim 85$ MPa, resulting in $\Delta n_{1.5,45^\circ} \sim 15$. At sufficiently high applied stresses, the dislocations can glide through the inclined shoulder part of the tension sample (Fig. 5b) to accomplish the given deformation. To further hinder this deformation, the cross-sectional area of the shoulder part of the sample was increased using the 90° flanks (Fig. 5c), therefore further lowering the stresses present in the sample heads. Consequently, higher flow stresses were determined for this sample. Taking a value of and $\Delta\tau_{1.5,90^\circ} \sim 160$ MPa evaluates $\Delta n_{1.5,90^\circ} \sim 30$. Notably, a similar number of dislocations is required in the pile-up of tension samples with $a = 1.5\ \mu\text{m}$ and $a = 8\ \mu\text{m}$, but is confined to a shorter glide plane length for the smaller specimen. This causes an increasing back-stress on the operating sources, explaining the high flow stress values. From the current understanding, this system should exhibit continuous hardening. Nevertheless, in the experiments a plateau value is reached for the small samples. A possible explanation for this behavior is cross-slip of dislocations [16], but to confirm this assumption, further investigations are required.

It is interesting to compare the present results to micro-compression testing. For example, single-crystal copper columns with an $\langle 1\,1\,1\rangle$ surface normal and a fixed aspect ratio of 2:1 have been compressed using the same in situ setup. Flow stresses from ~280 MPa to ~870 MPa were determined for diameters ranging from 8 μm to 1 μm at a strain of 20% [17]. Similar strong size effects have also been reported for single slip oriented materials; see for example Ref. [1]. These values [1,17] are significantly higher than those found in our miniaturized tensile tests for samples with high aspect ratios. We therefore speculate that the constraints in the deformation by the flat punch and the underlying substrate result in the formation of extensive dislocation pile-ups, which become responsible for the high flow stresses observed in micro-compression testing.

5. Summary and conclusions

- A method to perform in situ tensile testing of miniaturized specimens was developed. This provides the possibility to remove several dimensional constraints present in miniaturized compression testing.
- Single-crystal copper tension samples with diameters ranging from 0.5 μm to 8 μm and aspect ratios between 1:1 and 13.5:1 were loaded along the $\langle -2\,3\,4\rangle$ direction and a size dependence of the flow stress was observed.
- Tension samples with high aspect ratios (>5:1) exhibited single slip deformation, negligible hardening, and a moderate dependence of the flow stress on the sample size.
- Load drops in the stress–strain curve along with the corresponding appearance of distinctive glide steps during in situ monitoring lead to the statement that deformation is controlled by a single source for a certain strain increment. The weak size dependence of the flow stress at constant aspect ratio is attributed to the size of the dislocation sources governing plastic deformation.
- Samples with low aspect ratios (1:1) exhibited a pronounced size effect on the flow stress and significant hardening. This is explained by the formation of a dislocation pile-up.

Acknowledgement

Financial support by the Materials Center Leoben under the frame of the Austrian Kplus Competence Center Programme and the Austrian Fonds zur Förderung der wissenschaftlichen Forschung, Project P17375-N07, is gratefully acknowledged.

Appendix. Remarks to the experimental results

The present investigation advances far beyond conventional small-scale tensile testing. As a consequence, several experimental details had to be considered in advance or demand further discussion.

Does the weight of the sample head influence the experiments?

To avoid any bending of the tension sample due to the weight of the sample head, the bending stresses must not exceed the critical flow stress of single-crystal copper, which is in the order of 1 MPa for macro samples [15]. Therefore, the maximum surface stress due to bending for the used sample geometry was calculated. As a worst-case approximation, a bending length of 20 times the sample thickness was assumed, which is significantly longer than in our experiments. This results in a maximum stress at the surface of only 1×10^{-3} MPa. It is acknowledged that this is only a static estimation, and any dynamic effects must be avoided during sample handling and testing.

Does FIB preparation influence our results?

Previous investigations [3] pointed out the presence of a damaged layer with a thickness of several tens of nanometers on the surface of FIB milled specimen. Frick et al. [18] suggested that with reduced sample size the ratio of damaged material increases, leading to a rise in flow stress. Depending on the thickness of the layer and assuming a simple composite model, the surface layer must be 7–12 times stronger than bulk copper to explain our results, which is rather unlikely. Furthermore, in this case the flow stress should drop significantly once the first glide steps occurred, which was not observed in our experiments. On the other hand, Bei et al. [19] argued that dislocations generated close to the surface during FIB milling determine the flow stress. These dislocation sources are small compared to the tested sample size and should lead to a size-independent flow stress given by the Orowan stress ($\tau_S \sim 115$ MPa and ~300 MPa for source sizes of 100 nm and 30 nm, respectively) to operate these sources. This is also in contradiction to our results.

Are we able to distinguish between noise and displacement bursts? What about the resulting error bars?

The limit of the sample dimensions that can be tested is given by the noise present in the experiments. It is crucial to ensure that the magnitude of load drops indicating dislocation bursts is significantly larger than the noise present in the measurement. Therefore, the whole SEM was placed on an active damping system. Nevertheless, the indenter is mounted on leaf springs in a vacuum environment, and therefore without air damping. This makes the system very sensitive to any kind of vibrations. In our case they stem from the turbo molecular pump of the SEM, which cannot be uncoupled from the actively damped system. The noise of the free moving indenter under vacuum conditions is in the order of 50 μN, but gets significantly reduced when sample and gripper get into contact. Furthermore, to reduce noise for the smallest specimen with an aspect ratio of 5:1, six parallel samples were fabricated and loaded at the same time.

At the end of every loading experiment the displacement was held constant for 30 s. The noise present during this time with sample and gripper being in contact was evaluated to determine the error bars given in Fig. 10. The lateral dimensions of the specimen were determined using the field emission SEM column of the FIB. Therefore, the sample was not tilted like in the usual dual beam working mode to avoid uncertainties due to the inclined view. Consequently, the error in lateral dimension is below 50 nm.

What happens at the beginning of the load–displacement curve?

One aspect to be discussed is the initial part of the loading curve. Despite the nonlinear contribution due to surface roughness, it is still questionable what causes a rise in force of 0.04 mN over a length of ~300 nm in Fig. 3a. From visual observation as well as analysis of the noise present in the load–displacement data, it is clear that there was still a slit between sample and gripper. If the approach was aborted and the sample gripper moved back to its initial position, the load also reduced to the starting level. Charging of the gripper causes an electrostatic repel between sample and gripper, moving back the gripper in the x-direction. This causes a deflection of the leaf springs which is detected as load. After the first contact, both parts are at the same potential and no repelling forces are observed. This gets further supported by the fact that the contrast in the SEM changes once contact between the two parts is established. Considering sample and gripper as plate capacitor, a potential of ~40 V would support sufficient energy to explain the observed effect.

Why are there different initial loading slopes?

There are two major issues for different linear loading slopes. It was already mentioned that one can never achieve a perfect fit between the flanks of sample and gripper. Therefore, one can expect a steeper linear loading slope for any reload cycle (see Fig. 3b). This even holds true if the sample was handled and FIB milled between the two loading steps, as can be seen in Fig. 8. The flanks of sample and gripper were already in contact during the loading of the thicker sample, the surfaces are well adapted. Consequently, the pre-strained sample has a steeper, more linear loading slope compared to the unstrained sample. Additionally, one has to mention that the stiffness of the testing machine was not accounted for.

The second aspect is depicted in Fig. 6, which presents a decreasing loading slope for increasingly constrained tension samples. For samples with an aspect ratio of 1:1, dislocation glide is hindered by the sample geometry. Dislocations cannot reach the sample surface as they pile-up at the flanks (see Fig. 14a). This generates a back-stress and requires the activation of other sources and probably also glide systems with a smaller Schmid factor. Therefore, the geometrically confined samples have higher flow stresses than the unconstrained samples. This is also observed in Fig. 9 for samples with $a = 8$ μm.

It is acknowledged that bending of the samples would also decrease the loading slope. This would be more pronounced for samples with low aspect ratios, as the short sample length leads to higher bending angles. As mentioned previously, we leveraged the visual control provided by the in situ setup to carefully align sample and gripper in order to minimize this influence.

Is the stiffness of all other involved parts sufficient to ensure accurate determination of strains?

The accurate determination of sample strains requires sufficient stiffness of all involved parts (like copper needle or tungsten gripper). Moser et al. [20] showed the difference between strain calculated simply from piezo-displacement and determined properly by image correlation for their in situ micro-compression tests. It is also acknowledged that they used a setup with a rather low stiffness. In our case, the displacement is measured at the indenter tip. Furthermore, after unloading (Fig. 4f), the sample stayed in position, indicating that only the tensile sample was uniaxially deformed. No plastic deformation of any other involved part was detected.

References

[1] Uchic MD, Dimiduk DM, Florando JN, Nix WD. Science 2004;305:986.
[2] Zhang H, Schuster BE, Wei Q, Ramesh KT. Scripta Mater 2006;54:181.
[3] Kiener D, Motz C, Rester M, Dehm G. Mater Sci Eng A 2007;459:262.
[4] Motz C, Schöberl T, Pippan R. Acta Mater 2005;53:4269.
[5] Kiener D. PhD thesis, Montanuniversität Leoben, Austria.
[6] Fleck NA, Muller GM, Ashby MF, Hutchinson JW. Acta Metall Mater 1994;42:475.
[7] Kiener D, Rester M, Scheriau S, Yang B, Pippan R, Dehm G. Int J Mat Res 2007;98:1047.
[8] Nix WD, Gao H. J Mech Phys Solids 1998;46:411.
[9] Foreman AJE. Phil Mag 1967;15:1011.

[10] Nabarro FRN. Theory of crystal dislocations. Oxford: Clarendon Press; 1967.
[11] Hirth JP, Lothe J. Theory of dislocations. New York: Wiley; 1982.
[12] Parthasarathy TA, Rao SI, Dimiduk DM, Uchic MD, Trinkle DR. Scripta Mater 2007;56:313.
[13] Hull D, Bacon D. Introduction to dislocations. Oxford: Elsevier Butterworth-Heinemann; 2004.
[14] Dewald DK, Lee TC, Robertson IM, Birnbaum HK. Scripta Metall 1989;23:1307.
[15] Diehl J. Zugverformung von Kupfer-Einkristallen 1. Z Metallkd 1956;47:331.
[16] Kocks UF, Mecking H. Prog Mater Sci 2003;48:171.
[17] Kiener D, Motz C, Schöberl T, Jenko M, Dehm G. Adv Eng Mater 2006;8:1119.
[18] Frick CP, Orso S, Arzt E. Acta Mater 2007;55:3845.
[19] Bei H, Shim S, George EP, Miller MK, Herbert EG, Pharr GM. Scripta Mater 2007;57:397.
[20] Moser B, Wasmer K, Barbieri L, Michler J. J Mater Res 2007;22:1004.